the temporal evolution.

Our measurements were made to verify the theoretical relation (*2*) between normal velocity and curvature. The experimental data yield a diffusion coefficient, 2×10^{-5} cm^2/s, which is a good approximation of the diffusion coefficient of the autocatalytic species $HBrO_2$ and is comparable to the values given in (*15, 16*), $D_{KClO_4} = 1.79 \times 10^{-5}$ cm^2/s (*17, 18*).

REFERENCES AND NOTES

1. R. J. Field and M. Burger, Eds., *Oscillations and Traveling Waves in Chemical Systems* (Wiley-Interscience, New York, 1985).
2. C. Vidal and P. Hanusse, *Int. Rev. Phys. Chem.* **25**, 1 (1986).
3. J. Ross, S. C. Müller, C. Vidal, *Science* **240**, 460 (1988).
4. J. P. Keener and J. J. Tyson, *Physica* **21D**, 307 (1986).
5. J. P. Keener, *Soc. Ind. Appl. Math. J. Appl. Math.* **46**, 1039 (1986).
6. A. T. Winfree, *Science* **175**, 634 (1972).
7. R. J. Field, E. Körös, R. M. Noyes, *J. Am. Chem. Soc.* **94**, 8649 (1972).
8. R. J. Field and R. M. Noyes, *J. Chem. Phys.* **60**, 1877 (1974).
9. J. J. Tyson, in (*1*), pp. 93–144.
10. V. S. Zykov, *Biophysics* **25**, 329 (1980).
11. ———, *ibid.*, p. 906.
12. The mixture contains 48 m*M* sodium bromide, 340 m*M* sodium bromate, 95 m*M* malonic acid, and 380 m*M* sulfuric acid. A few minutes after these components are mixed the solution becomes colorless. Then ferroin is added (final concentration, 3.5 m*M*). This solution (3.6 ml) is transferred to an optically flat petri dish. The resulting thickness in the observation area of the dish is 0.5 to 0.6 mm. The measurements were performed at room temperature (24° ± 1°C) [S. C. Müller, Th. Plesser, B. Hess, *Science* **230**, 661 (1985)].
13. The sample layer is illuminated with diffuse light filtered with an interference filter of 490-nm peak transmittance, which corresponds to the maximum absorption of the catalyst ferroin. An inverse microscope is connected to a video camera with an image raster resolution of 512 × 512 picture elements. The maximum resulting resolution is 0.7 mm per picture element. Either single images with an intensity resolution of 256 gray levels at 2-s intervals or video movies with reduced spatial and intensity resolution at a frequency of 25 images per second can be recorded [S.C. Müller, Th. Plesser, B. Hess, *Anal. Biochem.* **146**, 125 (1985)].
14. S. C. Müller, Th. Plesser, B. Hess, *Naturwissenschaften* **73**, 165 (1986).
15. L. Kuhnert, H.-J. Krug, L. Pohlmann, *J. Phys. Chem.* **89**, 2022 (1985).
16. R. J. Field and R. M. Noyes, *J. Am. Chem. Soc.* **96**, 2001 (1974).
17. R. C. Weast, Ed., *Handbook of Chemistry and Physics* (CRC Press, Boca Raton, FL, ed. 60, 1979), p. F-62.
18. So far, we have confirmed the predicted relation (*2*) by observing areas of high negative curvature. Work is in progress to investigate propagating waves with high positive curvature to provide evidence for the predicted decrease is velocity due to the increase in curvature and to establish the existence of a minimum radius necessary for the onset of outward propagation of circular waves. With our data for *D* and *c*, this minimum radius is estimated to be 20 μm.

19. Fruitful discussions with J. J. Tyson and Zs. Nagy-Ungvarai are acknowledged. We thank U. Heidecke for laboratory assistance, K.-H. Müller for help with the computations, and A. Rohde for typing the manuscript. Supported by the Stiftung Volkswagenwerk, Hannover.

9 March 1988; accepted 6 June 1988

July Temperatures in Europe from Pollen Data, 6000 Years Before Present

Brian Huntley and I. Colin Prentice

Mean July temperatures across Europe 6000 years before present were reconstructed from palynological data by the transfer function method. Reconstructed summer temperatures were warmer than those at present over most of Europe with the greatest heating, more than 2°C, in the midcontinent and the far north. This pattern is explained by high summer insolation and a weak zonal insolation gradient 6000 years before present and the effective heating of the landmass relative to ocean and coastal areas. A strong land-sea pressure gradient may in turn have increased westerly air flow into southern Europe, which is consistent with cooler reconstructed summer temperatures in the Mediterranean region, and reduced the environmental lapse rate in the central European mountains.

Maps based on the changing relative abundances of taxa in fossil pollen records have shown that continental-scale vegetation patterns responded in a coherent way to long-term climatic changes during the past 10,000 to 20,000 years (*1–4*). In this report we use transfer functions, as developed by Webb and co-workers (*5–8*), to reconstruct mean July temperatures for 6000 years before present (B.P.) from European palynological data (*1*). Our study is part of the Cooperative Holocene Mapping Project (COHMAP), in which paleoclimate reconstructions based on palynological and other geological evidence (*4–7, 9*) have been compared to atmospheric general circulation model (GCM) simulations with global boundary conditions (insolation, ice sheets, sea-surface temperatures, and CO_2) appropriate to past times (*10, 11*).

The mean annual temperature gradient in Europe trends north-south, paralleling the gradient of annual insolation. The prevailing westerlies superimpose an east-west temperature and precipitation gradient with cool summers, warm winters, and high pre-

B. Huntley, Department of Botany, University of Durham, Science Laboratories, South Road, Durham, DH1 3LE, England.
I. C. Prentice, Institute of Ecological Botany, Uppsala University, Box 559, S-751 22 Uppsala, Sweden.

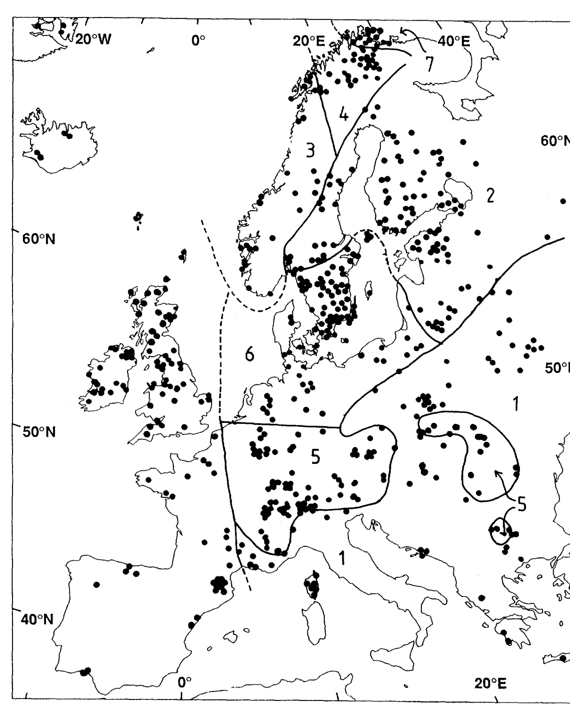

Fig. 1. Surface pollen samples used in the transfer function equations and calibration regions. Subregion 1 represents the gradient from Mediterranean sclerophyll vegetation through mixed-deciduous forest, bounded by the 17.5°C July isotherm. Subregion 2 represents the gradient from mixed-deciduous forest through northern/montane boreal forest and lies between the 17.5°C and 13.5°C July isotherms, excluding montane regions south of 51°N and the oceanic region west of the −4.5°C January isotherm. Subregion 3 represents the gradient from continental to oceanic boreal and mixed-deciduous forest and extends from the 13.5°C July isotherm to the Norwegian coast, including southern Norway west of 10°E but excluding northern Fennoscandia east of 18°E. Subregion 4 represents the gradient from boreal forest through sub-arctic *Betula* forest and extends east of 18°E from the 13.5°C July isotherm to the 11.5°C July isotherm, the approximate northern limit of *Pinus*. Subregion 5 represents the gradient from mixed-deciduous forest south of 51°N upwards from 17.5°C through the montane forest belts. Subregion 6 represents the same July temperature range as subregion 2, west of the −4.5°C January isotherm but excluding the most oceanic area in southern Norway. Subregion 7 represents the gradient north of the 11.5°C July isotherm from sub-arctic forest to shrub-tundra on the Arctic coast.

Table 1. Transfer function regression coefficients (b_i) and power terms (a_i) by subregion. Pollen sums are: subregion 1, *Abies, Alnus, Betula, Carpinus, Corylus, Fagus, Picea, Quercus* (deciduous and evergreen), *Tilia, Ulmus, Ostrya, Olea, Pistacia, Phillyrea*; subregion 2, *Alnus, Betula, Carpinus, Corylus, Fagus, Picea, Pinus, Quercus*; subregion 3, *Alnus, Betula, Corylus, Picea, Pinus, Quercus*; subregion 4, *Alnus, Betula, Juniperus, Picea, Pinus, Salix*, Cyperaceae, Gramineae, Ericales.

Taxon	Subregion 1		2		3		4	
	b_i	a_i	b_i	a_i	b_i	a_i	b_i	a_i
Alnus	−0.40	0.5	+0.06	1.0	+0.30	0.5		
Betula	−1.04	0.25	−2.33	0.25				
Fagus	−0.26	0.5						
Picea	−0.08	0.5	−0.06	1.0	+0.03	1.0		
Pinus			−1.68	0.25			+0.35	0.5
Quercus (deciduous)			+0.15	1.0	+0.86	0.5		
Quercus (evergreen)	−0.10	0.5						
Ostrya	+0.08	1.0						
Olea + *Pistacia* + *Phillyrea*	+0.23	0.5						

Table 2. Transfer function parameters by subregion.

Sub-region	b_0 (°C)	Number of observations	R^2	Standard error (°C)	July temperature range (°C)
1	23.6	68	0.90	0.8	17.5–26.0
2	26.0	98	0.48	0.8	13.5–17.5
3	11.1	26	0.81	0.5	11.5–15.5
4	10.6	29	0.82	0.2	11.5–13.5

cipitation toward the Atlantic Ocean. In summer the westerlies track north of the Mediterranean region and create a summer-dry Mediterranean climate (*12*). These climatic patterns are reflected in the distribution of vegetation and in surface pollen (*13, 14*), despite long and widespread human impact on European vegetation. Vegetation changes from tundra in the north to subarctic *Betula* (birch) and *Pinus* (pine) forests, boreal forests, temperate mixed-deciduous forests, and Mediterranean vegetation characterized by sclerophyll trees and shrubs in the south. *Picea* (spruce) is abundant in the boreal forest in the northeast; steppe replaces mixed-deciduous forest in the southeast. Forests with *Picea*, *Fagus* (beech), and *Abies* (fir) occur at middle elevations in the mountainous areas of central and southern Europe.

European vegetation was significantly different 6000 years ago (*13*). Mixed-deciduous forests extended higher and farther north than they do today. Sub-arctic *Pinus* and *Betula* forests also extended farther north, with *Betula* replacing tundra vegetation near the Arctic coast. The mixed-deciduous forests differed in composition, with more *Ulmus* (elm) and *Tilia* (lime) and less *Fagus* and *Carpinus* (hornbeam) than occurs today. *Picea* forests were confined to the northeastern part of the region; *Pinus* and *Betula* were abundant to the west of these forests. Montane forests with *Picea*, *Fagus*, and *Abies* were confined to the Balkans. There was no steppe, and "Mediterranean" vegetation was restricted to the Near East. These differences can be explained qualitatively by postulating that: (i) summers were warmer than they are today in central and northern Europe; (ii) winters were colder in northwest, central, and possibly southern Europe but warmer with less reliable snow cover than occurs today in northern Europe; (iii) precipitation was higher in eastern Europe; and (iv) the summer drought period was shorter (implying lower temperatures or higher precipitation or both during the growing season) in the Mediterranean region (*12, 15*).

We have quantified and mapped the differences in summer temperature between 6000 B.P. and the present using pollen-climate transfer functions. The transfer function model is:

$$C_k = b_0 + \sum_{i=1}^{n} b_i \cdot p_{ik}^{a_i} + e_k \qquad (1)$$

where C_k is the value of the climate variable at site k; p_{ik} are the pollen percentage values of n pollen types; b_0, b_i, and a_i are parameters that are estimated from contemporary (surface) pollen and modern climate data; and e_k is random error. The exponents a_i are required to linearize the relations between pollen abundance values and the climate variable. We estimated the a_i subjectively by inspecting graphical representations for a_i = 0.25, 0.5, and 1.0. We then fitted Eq. 1 by multiple linear regression onto the transformed pollen values (*16*).

Several articles have discussed the assumptions of transfer functions (*3, 4, 6, 8*). The most fundamental are (i) that there are quantitative relations between pollen abundances and climate variables and that these relations reflect a causal relation, however indirect; and (ii) that changes in pollen abundance reflect climatic changes. Other factors that influence vegetation composition are neglected. These assumptions are reasonable when examining first-order patterns of change across the continent over a period long enough for major changes in insolation and atmospheric circulation to have occurred. Transfer functions must satisfy the assumptions of the multivariate linear regression model. The residuals must be approximately normally distributed and homoscedastic and must not show spatial autocorrelation (*8*). We verified that these statistical assumptions were reasonable in our model by inspecting normal probability plots and scatter plots of the residuals against the climate variable, latitude, longitude, and elevation. We also used Cook's-distance plots (*8*) to check that the predicted climate values were stable when individual data points were excluded. This check guards against spurious regressions dominated by a few outlying points and eliminates the need to divide the modern data into training and test sets (*9*).

One limitation of the transfer function method is that a region as large as a continent is unlikely to yield monotonic relations between pollen abundances and climate (*4*). A large region usually has to be partitioned into climatic subregions, each with a different characteristic range of pollen assemblages (*4, 8*). Convenient boundaries between subregions commonly fall near abundance modes for major pollen taxa, but their precise location is subjective. We therefore experimented with different positions for the boundaries and with different numbers of subregions and we examined scatter plots of pollen abundance versus July mean temperature to identify those subregions that best met the criterion of monotonic relations. We eventually defined seven subregions within the window 4°E to 32°E and 35°N to 72°N (Fig. 1) and constructed separate transfer functions for each subregion using a network of surface pollen samples (*1, 17*) and an estimate of modern July temperature at each sample location (*18*). Then, for each 6000 B.P. sample, we located the three most similar surface samples by the chord-distance criterion (*19*). This gave an initial basis for deciding which transfer function to apply. We made final assignments using the iterative procedure developed by Bartlein and Webb (*8*). These assignment procedures resulted in only four out of the seven equations being used for the final reconstruction (Tables 1 and 2), and these equations were used over areas that were significantly different from the original subregions (Fig. 2). The changes reflect the considerable changes in the extent and location of vegetation regions since 6000 B.P. (*13*).

Differences between reconstructed (6000 B.P.) and present July mean temperatures (Fig. 3) have a strong regional variation. The differences are consistently larger than the nominal standard errors (Table 2) (*20*) at multiple sites in a region. The reconstruction indicates that July temperatures were warmer than those today over most of Europe (by about 2°C in the midcontinent). The latitudinal gradient was reduced (*21*), with July temperatures >2°C warmer than they are at present in the far north but cooler than at present around the Mediterranean. Areas of high elevation in central Europe may have been warmer by as much as 5°C (*22*). These results generally agree with the classical idea of a mid-Holocene thermal maximum in central and northern Europe (*23*), but the temperature difference (Fig. 3) varies considerably in space and July temperatures were apparently cooler than at present at low elevations in southern Europe (*21*).

Plausible mechanisms that may be invoked to explain climatic differences between 6000 B.P. and today include the response of the general atmospheric circulation to orbitally induced changes in the seasonal and latitudinal distribution of insolation and the response of mesoscale climatic processes to these circulation changes. The first mechanism can be tested by a comparison of the reconstruction with GCM results for simulations that change only the amount and distribution of insolation; the second mechanism cannot be tested until accurate mesoscale climate models become available.

Quasi-periodic changes in mid- to high-latitude insolation are well known to have paced the growth and decay of the Northern Hemisphere ice sheets (*24*), and changes in insolation also caused direct, immediate climatic responses [for example, in summer temperatures at high latitudes (*25*) and in tropical monsoons (*26*)] that were independent of the effects of late Quaternary insolation changes on the ice sheets (*27*). At 70°N, July insolation at 6000 B.P. was ≃7% greater than it is today, but it was only ≃5% greater at 30°N (*10*). We might therefore have expected that, compared to current conditions, summers would have been generally warm and the north-south summer temperature gradient reduced at 6000 B.P. The different thermal capacity of land and water and the transfer of heat between them must also be taken into account (*10*). A GCM experiment (*10, 28*) (with prescribed sea-surface temperatures similar to those today) has indicated not only that increasing July insolation to match conditions 6000 years ago should have caused temperature increases of 1° to 2°C in Europe, but also that the warming should have been greatest in the midcontinent and less in coastal regions, including the region around the Mediterranean. Thus we interpret much of the pattern in Fig. 3 to reflect the combined effects of altered summer insolation and the differential heating of the landmass; the approximate magnitude of the anomaly and

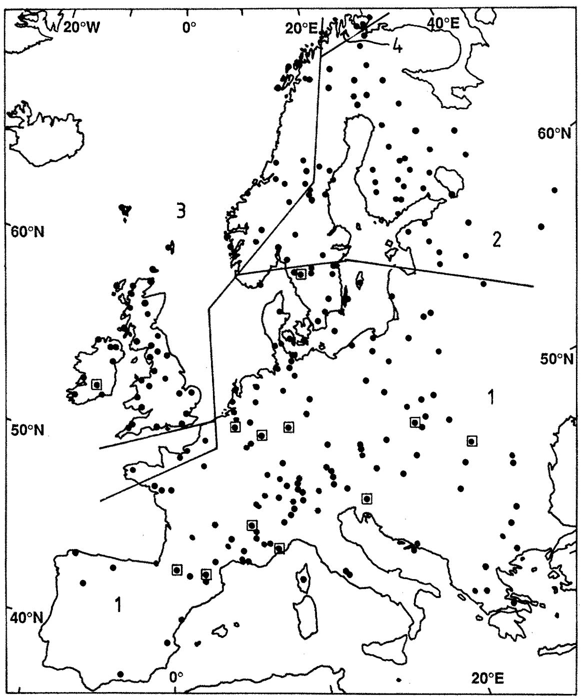

Fig. 2. Locations of the 6000 B.P. palynological sites. Sites shown in boxes had minimum squared chord-distance values more than 0.15 higher than the values for nearby sites; these were considered anomalous and omitted from the reconstruction. The regions outlined are those within which each of the calibration equations was applied. No reconstruction was made for the sites in northernmost France (*20*).

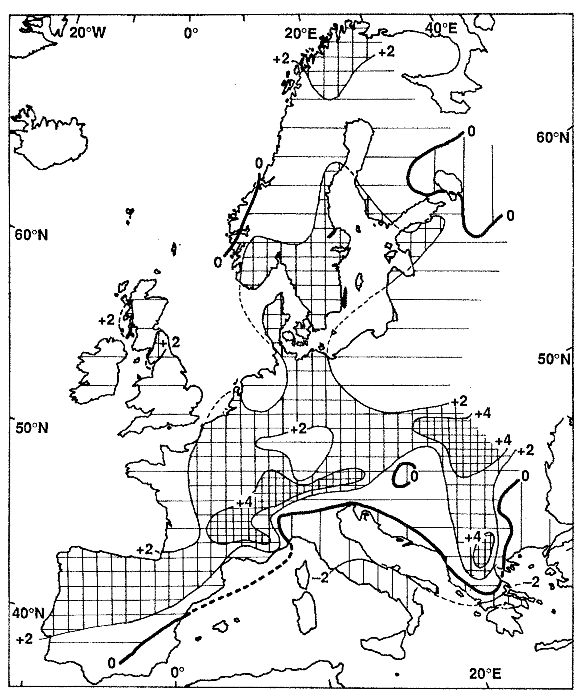

Fig. 3. Reconstruction of the July mean temperature anomaly pattern at 6000 B.P. The isotherms are for 6000 B.P. minus present.

the broadest features of its spatial pattern are in agreement with the GCM experiment.

The same GCM experiment (*10, 28*) produced significant negative sea-level pressure anomalies over continental Europe and North Africa. Compared to current conditions, these anomalies would have increased westerly air flow into southern Europe; this flow in turn would have increased orographic precipitation and thus produced cooler and moister summers at low to moderate elevations. The large increases in average July temperature reconstructed for high elevations might also be explained by more frequent incursions of moist air into the central European mountains, because at any given altitude the moist adiabatic lapse rate would then apply for a greater proportion of the growing season (*29*). This effect could conceivably have lowered the mean environmental lapse rate in summer by as much as 1°C km^{-1}, enough to produce the strong differential heating suggested by the results in Fig. 3.

REFERENCES AND NOTES

1. B. Huntley and H. J. B. Birks, *An Atlas of Past and Present Pollen Maps for Europe: 0–13,000 Years Ago* (Cambridge Univ. Press, Cambridge, 1983).
2. G. M. Peterson, thesis, University of Wisconsin–Madison (1983); J. C. Bernabo and T. Webb III, *Quat. Res. (N.Y.)* **8**, 64 (1977); M. Ralska-Jasiewiczowa, *New Phytol.* **94**, 133 (1983).
3. T. Webb III, *Vegetatio* **67**, 75 (1986).
4. I. C. Prentice, *Progr. Phys. Geogr.* **7**, 273 (1983).
5. S. Howe and T. Webb III, in *Fifth Conference on Probability and Statistics* (American Meteorological Society, Boston, 1977), pp. 152–157.
6. ——, *Quat. Sci. Rev.* **2**, 17 (1983).
7. P. J. Bartlein, T. Webb III, E. C. Fleri, *Quat. Res. (N.Y.)* **22**, 361 (1984).
8. P. J. Bartlein and T. Webb III, *Syllogeus* **55**, 301 (1985).
9. T. Webb III and R. A. Bryson, *Quat. Res. (N.Y.)* **2**, 70 (1972).
10. J. E. Kutzbach and P. J. Guetter, *J. Atmos. Sci.* **43**, 1726 (1986).
11. T. Webb III, P. J. Bartlein, J. E. Kutzbach, in *North America and Adjacent Oceans During the Last Deglaciation*, W. F. Ruddiman and H. E. Wright, Jr., Eds., vol. K-3 of *The Geology of North America* (Geological Society of America, Boulder, 1987), pp. 447–462.
12. B. Huntley and I. C. Prentice, in *Global Climates*, COHMAP Members, J. E. Kutzbach, W. A. Ruddiman, F. A. Street-Perrott, T. Webb III, H. E. Wright, Jr., Eds. (Univ. of Minnesota Press, Minneapolis, in press).
13. B. Huntley, in *Vegetation History*, B. Huntley and T. Webb III, Eds. (Kluwer, Dordrecht, in press).
14. ——, unpublished discriminant analysis; results (B.H.) show that groups of surface samples classified on the basis of their quantitative pollen composition can be discriminated with simple meteorological data for their localities.
15. COHMAP Project Members, *Science*, in press.
16. In this study, the maximally predictive subset among all possible subsets of the pollen variables was chosen as the subset with the lowest value of Mallows' C_p, given by:

$$C_p = \frac{SSE_p}{s^2} - (N - 2p)$$

where p is the number of variables in the model including the intercept, N is the number of observations, SSE_p is the sum-of-squares error for a model with p variables, and s^2 is the mean square error for the full model. This statistic quantifies the trade-off between increasing R^2 and decreasing prediction accuracy as the number of variables is increased. See S. Weisberg, *Applied Linear Regression* (Wiley, New York, ed. 2, 1985).
17. G. M. Peterson, *Quat. Sci. Rev.* **2**, 281 (1984); I. C. Prentice, *J. Biogeogr.* **10**, 441 (1983).
18. F. Steinhauser, *Climatic Atlas of Europe* (World Meteorological Organisation, Geneva, 1970), vol. 1.
19. J. T. Overpeck, T. Webb, III, I. C. Prentice, *Quat. Res. (N.Y.)* **23**, 87 (1985).
20. Initial boundaries that were based on the provenance of the modern analog samples were progressively adjusted until reconstructed temperatures on either side of any boundary were minimally affected by further change. The discrepancy between the alternative reconstructions for sites near the final boundaries was generally <0.5°C, but discrepancies of ≃2°C occurred in northernmost France and in a narrow zone on the steep temperature gradient across the Scandes. The remaining uncertainty in placing the boundaries means that errors in the reconstructed temperatures can be somewhat larger than is implied by the standard errors for the individual regression equations (Table 2), especially near the boundaries and in areas of high relief.
21. A reduced, mid-Holocene latitudinal gradient of summer temperature was also reported by Grichuk [M. P. Grichuk, in *Golotsen*, M. I. Neishtadt, Ed. (Idz-vo Nauka, Moscow, 1969), pp. 41–57] on the basis of an indicator-species method applied to a much smaller number of sites.
22. Guiot [J. Guiot, *Quat. Res. (N.Y.)* **28**, 100 (1987)], using a different form of the transfer function method, also found mid-Holocene July temperature anomalies of ≃5°C at high elevation sites in southern France.
23. J. Iversen, *Dan. Geol. Unders. Afh. Raekke 5* **7C**, 1 (1973).
24. J. Imbrie and J. Z. Imbrie, *Science* **207**, 943 (1980); J. D. Hays, J. Imbrie, N. J. Shackleton, *ibid.* **194**, 1121 (1976).
25. J. C. Ritchie, L. C. Cwynar, R. W. Spear, *Nature* **305**, 126 (1983).
26. J. E. Kutzbach, *Science* **214**, 59 (1981); M. Rossignol-Strick, *Nature* **304**, 46 (1983); J. E. Kutzbach and F. A. Street-Perrott, *ibid.* **317**, 130 (1985).
27. J. E. Kutzbach and P. J. Guetter, in *Milankovitch and Climate*, A. Berger, J. Imbrie, J. Hays, G. Kukla, B. Saltzman, Eds. (Reidel, Dordrecht, 1984), part 2, pp. 801–820.
28. ——, *Ann. Glaciol.* **5**, 85 (1984).
29. The moist adiabatic lapse rate is less than the dry adiabatic lapse rate because of the release of latent heat as water vapor in the moist air condenses during the cooling, which in turn results from expansion as the pressure of the body of air declines.

30. Natural Environment Research Council grant GR3/2877 and U.S. Department of Energy (DOE) grant DE-AC02-79-EV 10097 supported the data compilation; a University of Southampton Hartley Fellowship (to I.C.P.) and DOE grant DE-AC02-79-EV 10097 supported the climatic reconstruction. We thank H. J. B. Birks for his part in the development of the database; COHMAP project members at large for discussions throughout the project; and especially P. J. Bartlein, J. E. Kutzbach, and T. Webb III for encouragement and creative input. T. C. Atkinson, P. J. Bartlein, K. D. Bennett, J. C. Ritchie, J. Turner, W. A. Watts, and T. Webb III critically read earlier drafts.

2 February 1988; accepted 7 June 1988

The Titan −1:0 Nodal Bending Wave in Saturn's Ring C

PAUL A. ROSEN AND JACK J. LISSAUER*

The most prominent oscillatory feature observed in the Voyager 1 radio occultation of Saturn's rings is identified as a one-armed spiral bending wave excited by Titan's −1:0 nodal inner vertical resonance. Ring particles in a bending wave move in coherently inclined orbits, warping the local mean plane of the rings. The Titan −1:0 wave is the only known bending wave that propagates outward, away from Saturn, and the only spiral wave yet observed in which the wave pattern rotates opposite to the orbital direction of the ring particles. It is also the first bending wave identified in ring C. Modeling the observed feature with existing bending wave theory gives a surface mass density of ~0.4 g/cm² outside the wave region and a local ring thickness of ≲5 meters, and suggests that surface mass density is not constant in the wave region.

The Voyager 1 radio occultation profiles of Saturn's rings contain numerous wave-like features (*1*). We present strong evidence that the most prominent, previously unidentified, wave is a one-armed spiral bending wave excited by the gravitational potential of the satellite Titan at its −1:0 nodal inner vertical resonance (IVR) (*2*). Bending waves form when the periodic out-of-plane perturbations by a satellite in an inclined orbit and the self-gravity of the ring disk force particles near a resonance into locally coherent vertical oscillations, warping the plane of the rings into a corrugated spiral pattern (*3, 4*). A one-armed spiral bending wave arises at a nodal resonance, where the satellite perturbations act with a periodicity equal to that of the nodal regression rate of the ring particles. The wave propagates outward, away from Saturn. Its spiral pattern winds in a "leading" sense, that is, along the direction of motion of the particles; the pattern rotates, however, in a retrograde direction, against the particles' motion.

The Titan −1:0 nodal bending wave is

P. A. Rosen, Center for Radar Astronomy, Stanford Electronics Laboratories, Stanford University, Stanford, CA 94305-4055.
J. J. Lissauer, Astronomy Program, Department of Earth and Space Sciences, State University of New York, Stony Brook, NY 11794-2100.

*Alfred P. Sloan Research Fellow.